Original article

Nuclear Medicine Communications

Fourier block noise reduction: an adaptive filter for reducing Poisson noise in scintigraphic images

Matthew J. Guy

Objectives **Both qualitative and quantitative analysis in nuclear medicine can be undermined by Poisson noise in low-count clinical images. Whilst the conventional smoothing filters are typically used do reduce noise, they also degrade the image structure. Fourier block noise reduction (FBNR) is an adaptive filtering approach, which attempts to reduce image noise and maintain image resolution and structure.**

Methods **Although a degree of automated flexibility is possible using conventional stationary pre-filtering, e.g. using a total image count-dependent Metz filter, resolution and contrast is degraded across the image. Adaptive non-stationary filtering has been applied by others in an attempt to maintain structure whilst reducing noise: instead of analysing the whole image, only a subset is used to determine each pixel's correction. Whilst the new software algorithm FBNR shares some common components with other adaptive non-stationary filters, it expressly includes the Poisson noise model within a simple and robust algorithm that can be applied to a diverse range of clinical studies.**

Results and conclusions **No additional artefacts were seen post-application of FBNR during evaluation using simulated and clinical images. Mean normalised error values indicate FBNR processing is equivalent to obtaining an unprocessed image with at least 2.5 times the number of counts.** *Nucl Med Commun* **29:291–297 © 2008 Wolters Kluwer Health | Lippincott Williams & Wilkins.**

Nuclear Medicine Communications 2008, **29:**291–297

Keywords: diagnostic imaging, image filtering, Poisson noise

Department of Medical Physics, Royal Surrey County Hospital, Guildford, UK

Correspondence to Dr M.J. Guy, Department of Medical Physics, Nuclear Medicine, The Royal Surrey County Hospital, Guildford, Surrey, GU2 7XX, UK
Tel: +44 (0)1483 406709; fax: +44 (0)1483 406702;
e-mail: matthew.guy@nhs.net

Received 9 May 2007 **Revised** 30 July 2007
Accepted 9 October 2007

Introduction

Image quality in clinical nuclear medicine single photon emission computed tomography (SPECT) and planar imaging is limited by a range of factors, including scatter [1], attenuation [2], limited spatial resolution [3] and patient motion [4]. Progress on all of these aspects is easily undermined, however, by the high levels of noise typically found in clinical acquisitions. Even in a modern 'digital' gamma camera, the detected count statistics are dominated by the double stochastic Poisson distribution due to the randomness of radioactive decay and the electron counting statistics within the photomultiplier tubes. Because of this, the standard deviation of each pixel's count value is equal to the square root of the mean count. Therefore, low-count clinical images are subject to high levels of Poisson noise. Noise within each image is concentrated at high frequencies, where the true signal drops due to the limited spatial resolution of the camera [5].

Conventional pre-reconstruction filtering, such as applying the ramp–Hanning or Butterworth filter, have been widely shown to improve traditional filtered back-projection SPECT imaging, by reducing the amplification of the high-frequency image components and can also improve planar views. A degree of automated flexibility can be achieved using these stationary filters; for example, using a total-image count-dependent Metz filter [6] or an image-dependent Metz restoration [7]. These filters are applied globally across all image pixels and whilst they reduce noise they also degrade resolution and contrast across the whole image.

Adaptive non-stationary filtering has been applied to nuclear medicine imaging [8–10] in an attempt to maintain structure whilst reducing noise. Instead of analysing the whole image, only a subset of the image is used to determine each pixel's correction, such as proposed by Lee [11] in his noise reduction filter applied to synthetic aperture radar images. Of those referenced, only the statistical and heuristic image noise extraction (SHINE) algorithm, developed by Hannequin and Mas [10], specifically utilizes the Poisson nature of the image noise.

Although the results presented by Hannequin and Mas [10] are promising, the complete SHINE process is 'patent pending', potentially limiting its adoption by the wider nuclear medicine community and is, arguably, over-complex for routine clinical use. Therefore, a new software algorithm, known as Fourier block noise reduction (FBNR), has been developed which attempts to preserve

0143-3636

the structure of low-count nuclear medicine images, whilst significantly decreasing noise. Whilst it shares some common components with the adaptive non-stationary filters mentioned above, it expressly includes the Poisson noise model within a simple and robust algorithm that can be applied to a diverse range of clinical studies.

Methods and materials

Object and simulated images

Object images

A Williams liver phantom was filled with 260 MBq of ^{99m}Tc. One hundred and eighty-six dynamic frames were acquired using a 128×128 matrix (1.72 mm pixel) on a Toshiba GCA-7200A gamma camera. By selectively summing the acquired frames, the total image counts could be varied from 0.3×10^6 to 70.9×10^6, with corresponding maximum pixel values of 138 and 32 655, respectively.

Fig. 1

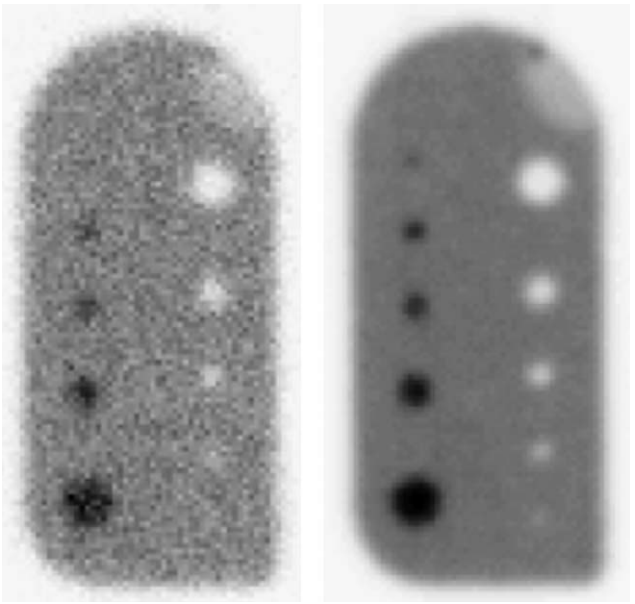

Planar Williams liver phantom images used for FBNR assessment. The minimum (left) and maximum (right) count density images are shown.

A Jaszczak phantom, with cold-sphere and rod inserts, was filled with 550 MBq of ^{99m}Tc. One hundred and twenty 30-s projections were acquired over 360° on the Toshiba GCA-7200A gamma camera. FBNR was applied to the raw projection data prior to ordered subset expectation maximization (OSEM) reconstruction using eight subsets, two iterations and attenuation correction ($\mu = 0.12\,\mathrm{cm}^{-1}$). No additional pre- or post-reconstruction filtering was applied (Fig. 1).

Simulation images

Three simulation phantom images were used to assess the performance of FBNR. They were not designed to mimic any specific clinical distribution but to evaluate the ability of the algorithm to maintain a range of structures compared to conventional methods. The three phantoms are shown in Fig. 2.

The uniform phantom is simply Poisson noise applied to the same global pixel value and was used to assess any detrimental changes in the image texture after noise reduction.

The block phantom consists of uniform square blocks of widths 1, 2, 3, 4, 5 and 6 pixels. Each dimension was repeated twice and each block was spaced 10 pixels apart. The background count level was set at 0.01 times the maximum (block) pixel value.

The line phantom consists of uniform horizontal and vertical lines spaced at 20 pixel intervals of width 1, 2, 3, 4, 5 and 6 pixels. The background count level was set at 0.25 times the maximum (line) pixel value.

Poisson noise was applied to all pixels for all phantoms. No other image degradation, for example scatter or point spread function, was included. Maximum pixel values of between 5 and 500 counts were simulated.

Fig. 2

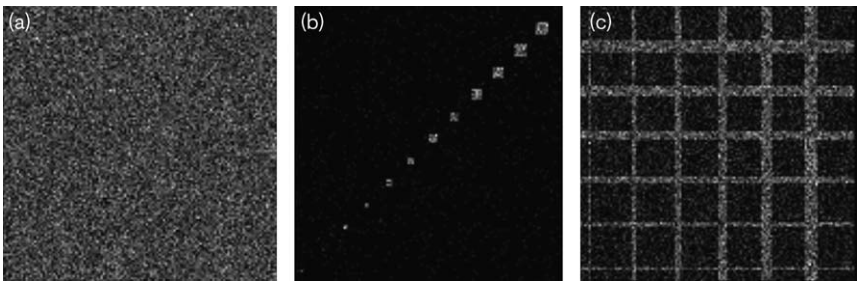

The uniform (a), block (b), and line (c) simulation phantoms used during this study. The maximum true pixel count in each image is 5.

Clinical images

Three-dimensional ^{123}I-DaTSCAN SPECT data is usually acquired to evaluate binding of the tracer in the caudate and putamen. However, for a particularly claustrophobic patient this protocol was not feasible and a vertex view 256×256 static dataset was acquired. The maximum pixel recorded in the caudate and putamen was 67.

A gated ^{99m}Tc-tetrofosmin myocardial perfusion SPECT study was also used to assess FBNR. Eight gated frames were acquired for each of the sixty 128×128 projections acquired over 180°. The maximum projection pixel count recorded was 66. Two datasets were formed: one using all the acquired data and the other using only half the acquired counts, with Poisson noise added to resemble a half-count acquisition. FBNR was applied to the half-count projection set. Both datasets were pre-filtered using a Butterworth filter (order 4, cut-off of 0.7 Nyquist) before applying filtered back-projection reconstruction. The QGS (Qualitative Gated SPECT, Cedars-Sinai Medical Center, California, USA) package was then used to view the datasets.

Conventional filtering

As well as comparing raw (Poisson noise) and FBNR images, each set of raw data was smoothed using a Hanning filter and a median filter. The median filter replaces each pixel's value with the median of its neighbours, in this case from the surrounding 3×3 values, and offers a limited degree of edge (structure) preservation, whilst the Hanning filter is commonly used in clinical imaging applications.

The clinical datasets were compared with the standard image filtering used for each type within the Nuclear Medicine Department at the Royal Surrey County Hospital.

Fourier block noise reduction formulation

Consider an $m \times m$ block within a digital image. For a 128×128 image, m is usually chosen to equal 4 or 8 pixels. This size corresponds to approximately equal (4×4) or double (8×8) the clinical FWTM system spatial resolution with low energy high resolution (LEHR) collimation. Within the sub-block the total variance (σ^2_{total}) is equal to the sum of the unknown signal variance (σ^2_{signal}) plus the variance due to noise (σ^2_{noise}):

$$\sigma^2_{\text{total}} = \sigma^2_{\text{signal}} + \sigma^2_{\text{noise}}. \qquad (1)$$

The total variance can be calculated using:

$$\sigma^2_{\text{total}} = \left[n \sum x^2 - \left(\sum x \right)^2 \right] / [n(n-1)] \qquad (2)$$

where $n = m \times m$, and $\sum x$ is the sum of all pixel values, x, within the sub-block.

As the noise within the $m \times m$ sub-block follows the Poisson model, σ^2_{noise} can be estimated to be equal to the mean pixel value within the sub-block. To check that this approximation can be justified, eighty 30-s frames of a Williams phantom were acquired (as previously described in Object Images). The σ^2_{noise} for each pixel was calculated by performing a gaussian fit to the count distribution. The σ^2_{noise} estimate from FBNR was also recorded and compared.

In the SHINE algorithm [10], estimation of the true signal is relatively complex and involves performing correspondence analysis. FBNR uses a far simpler approach. It is assumed that the majority of the noise within the sub-block is concentrated at higher frequencies [5]. The sub-block is passed through a low-pass cut-off filter (calculated by taking the FFT of the block and selectively rejecting high-frequency components) and the unknown signal (σ^2_{signal}) within the sub-block can be estimated ($\sigma^2_{\text{total}'}$) and compared with the original total variance. The resulting residual variance ($\sigma^2_{\text{residual}}$) is given as:

$$\sigma^2_{\text{residual}} = \sigma^2_{\text{total}} - \sigma^2_{\text{total}'} \qquad (3)$$

where $\sigma^2_{\text{total}'}$ is calculated from the estimated sub-block as in Equation 2.

If the current estimate of the residual variance, $\sigma^2_{\text{residual}}$, is equal to σ^2_{noise}, $\sigma^2_{\text{total}'}$ becomes equal to σ^2_{signal} (i.e., 'all' noise has been removed from the sub-block). Therefore, the cut-off frequency is increased until $\sigma^2_{\text{residual}} \leq \sigma^2_{\text{noise}}$ and $\sigma^2_{\text{total}'}$ is almost equal to the true signal variance σ^2_{signal}.

A three-stage approach is used to determine this cut-off frequency to the nearest 0.01 of the Nyquist frequency. This process is faster than searching for the optimum stopping condition over the entire frequency range (0 to Nyquist) and is outlined below.

Step 1. The frequency is determined iteratively to the nearest i/m-th of the Nyquist frequency, where i is an integer between 0 and $m-1$. As m is usually only 4 or 8 for clinical data, this first step results in a crude estimate of the cut-off frequency required.
Step 2. Once the initial stop condition, i, has been identified (where $\sigma^2_{\text{residual}} < \sigma^2_{\text{noise}}$), the process is then repeated allowing a fraction j of the signal over the frequency range $(i-1)/m$ to i/m of the Nyquist value to be included, where j has a value between 0 and 1. To begin with, fraction j is determined (by attempting to find $\sigma^2_{\text{residual}} = \sigma^2_{\text{noise}}$) to the nearest 0.1.
Step 3. Step 2 is then repeated at 0.01 intervals over the range $(j-0.1)$ to j. The optimum fraction of signal over the frequency range $(i-1)/m$ to i/m is therefore determined to the nearest 0.01.

Fig. 3

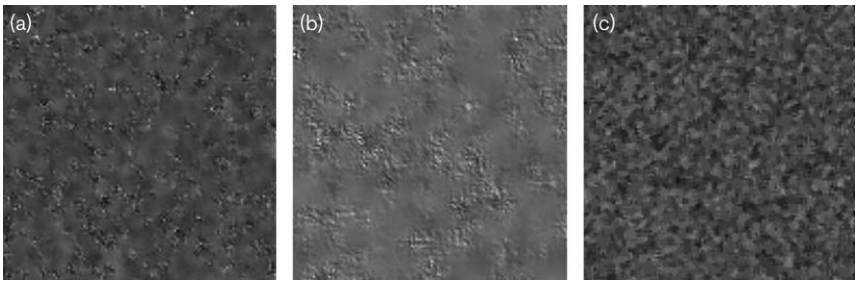

Processing of a simulated uniform count distribution with original pixel count of 5 following the addition of Poisson noise [as shown in Fig. 2(a)]. (a) FBNR with a 4×4 sub-block; (b) FBNR with a 8×8 sub-block; and (c) median filter applied.

Fig. 4

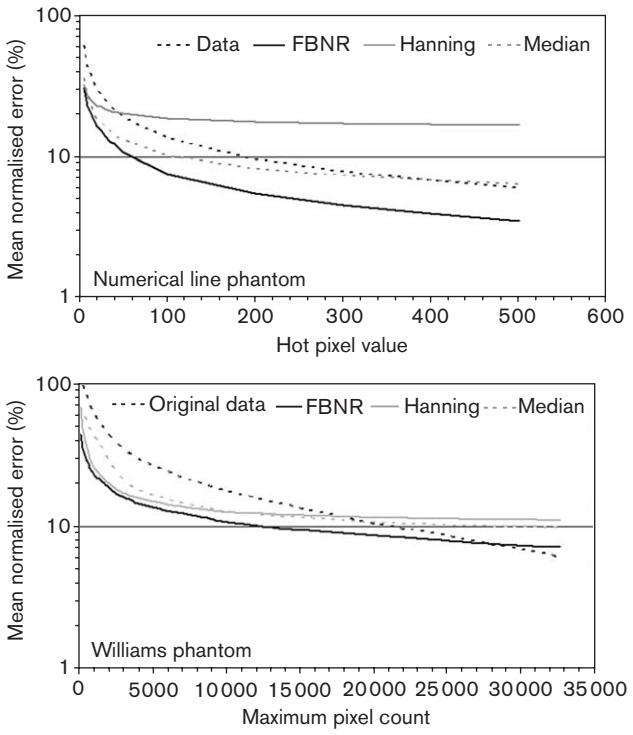

Mean normalised error values for (from top to bottom) the line, block and Williams phantoms. FBNR values using a 4×4 sub-block are shown.

Fig. 5

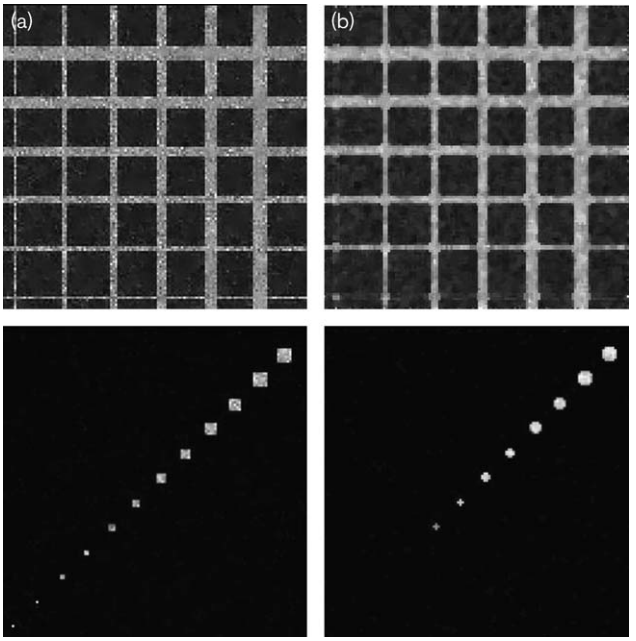

Comparison of (a) FBNR (4×4 sub-block) and (b) median-filtered images for the line (top) and block (bottom) numerical phantoms, with an original hot pixel level of 25 counts.

This simple process would be likely to cause unacceptable artefacts in the final image if the algorithm were applied block by block (i.e., stepping m pixels through the image): block-like artefacts would be visible at the edge of sub-blocks where the cut-off frequency changed significantly. Therefore, the sub-blocks are moved by just 1 pixel, as used by Hannequin and Mas [10], between calculations (first along the x-axis and then the y-axis): each pixel value is formed from the mean of $m \times m$ estimates. For example, for a 4×4 sub-block, each pixel's value is calculated by the sum of 16 estimates and then finally divided by 16 to maintain count normalization.

Fourier block noise reduction implementation

The FBNR program was written in IDL (ITT Visual Information Solutions, Boulder, Colorado, USA) and does not require any user intervention. As delayed acquisitions for radionuclide therapy dosimetry calculations can suffer from high noise levels, the algorithm has been included in the RMDP dosimetry package [12].

Evaluation

FBNR and the conventional filtering algorithms described in the last section were evaluated using the object, simulation and clinical data shown in the Materials and Methods section. In the case of the object and simulation studies, the mean normalized error (MNE) was calculated over the whole image. For a 128×128 image this is given by:

$$\mathrm{MNE} = \left(100/128^2\right) \sum \mathrm{ABS}(x' - x)/x \qquad (4)$$

where $\sum$ is the sum over all pixels in the image, x' is the estimated pixel count value and x is the known pixel count value.

Fig. 6

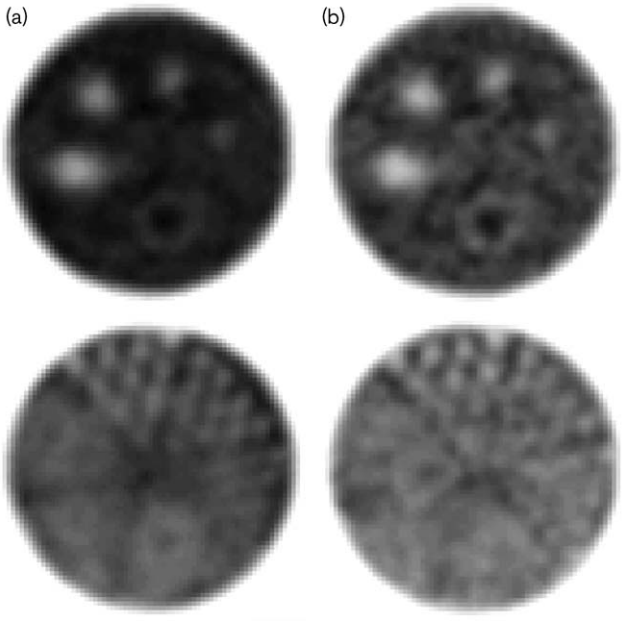

Comparison of (a) FBNR (4×4 sub-block) and (b) raw Jaszczak phantom transverse slices, showing the cold sphere (top) and rod (bottom) inserts.

For the Williams phantom data, the high-count distribution was assumed to be 'noise-free' and these scaled pixel values used to represent x. Block sizes of 4×4 and 8×8 pixels for 128×128 images were evaluated for FBNR.

A visual comparison of the raw and FBNR clinical datasets was made. A sub-block size of 4×4 was used for all datasets. With the exception of the numerical datasets, all images were displayed using a linear inverse grey-scale colour table.

Results and discussion

Object and simulation image evaluation

Comparison of the true and estimated $\sigma^2_{\mathrm{noise}}$ values for the Williams phantom showed that the 4×4 block FBNR estimate is acceptable and that the noise present in gamma camera images can be accurately represented by the Poisson model for clinical pixel values (with a correlation coefficient > 0.997 for pixel values up to 5000). No visible artefacts (i.e., structures) were seen in the $\sigma^2_{\mathrm{noise}}$ error map. The average pixel error within the phantom was less than 2%. The average absolute difference was found to be $10.6\% \pm 8.6\%$, with a maximum error in $\sigma^2_{\mathrm{noise}}$ of 36%. This relatively small level of discrepancy is due to the small image area occupied by each sub-block (typically $\sim 1\%$ or $\sim 4\%$ of the total area).

Visual assessment of the simulated datasets suggested a qualitative bias towards using a 4×4 block for 128×128 images when processing with FBNR, as this gave more 'natural' results, as shown in Fig. 3. Processing times with 4×4 compared to 8×8 sub-blocks are also reduced. The exact processing time required will depend on the count distribution within each image. Typical processing times per 128×128 pixel frame were found to be 7 s and 11 s for a 4×4 and 8×8 sub-block respectively (P4 2 GHz, 1 GB RAM). Further optimization to improve the efficiency of the current code is realistic and currently being developed.

Fig. 7

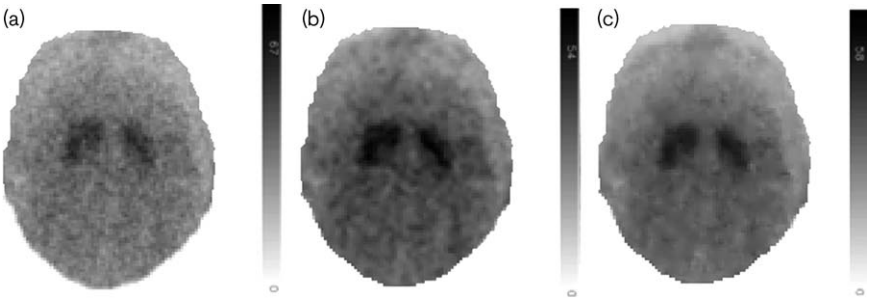

Comparison of (a) raw, (b) median-filtered and (c) FBNR (4×4 sub-block) vertex-view DaTSCAN data, after masking counts from torso and marker.

Fig. 8

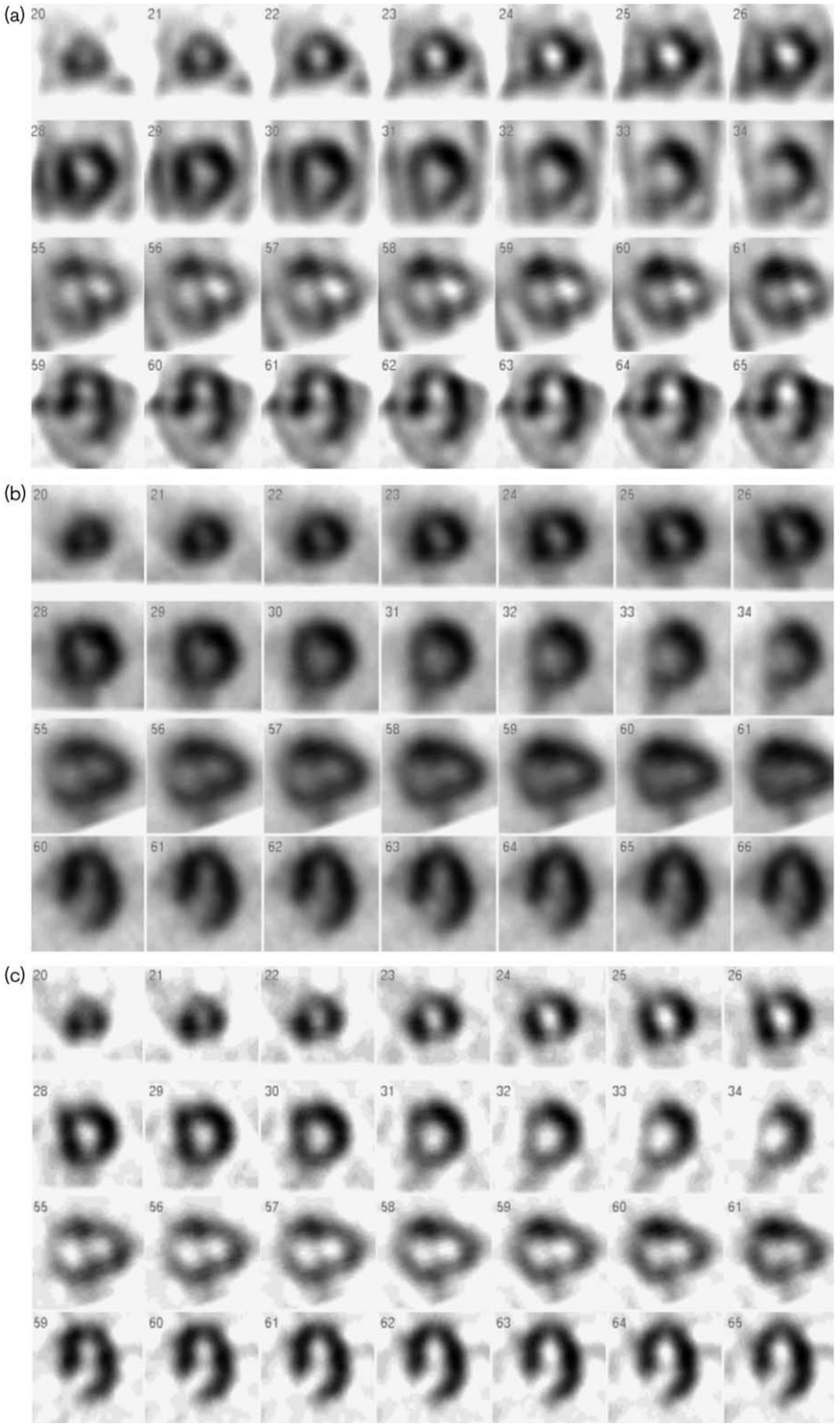

QGS output from a clinical MPS study: (a) half-count data, (b) original full-count data, (c) half-count data with FBNR. Each dataset was fully automatically processed in QGS and images reviewed using an inverse greyscale colour-map.

Quantitative assessment using the MNE for each whole image, demonstrated that the overall performance of both FBNR methods (4×4 and 8×8 sub-block) for all clinical pixel values (up to a maximum pixel value of 500 counts) used was superior to the conventional filters assessed here. As expected, the simple median filter was the worst performer in this count range. Sample MNE charts for the line, block and Williams phantoms are shown in Fig. 4. For the Williams phantom, FBNR out-performs Hanning filtering for the entire count range of the study. Significantly, its MNE is over 30% lower than that obtained by Hanning filtering for low (maximum pixel count of less than 150) count data and FBNR maintains this magnitude of improvement over a clinically realistic count range ($> 20\%$ improvement versus Hanning filtering up to a maximum pixel count of 500).

In addition to the favourable overall image quantification results, FBNR processing demonstrated an enhanced ability to maintain image contrast and resolution and shown in Figs 5 and 6 for the numerical and Jaszczak phantoms, respectively.

The addition of FBNR does not introduce any new artefacts into the Jaszczak data, although underlying artefacts caused by the poor uniformity stability of the gamma camera used during this study are visible on both datasets. Qualitatively, the FBNR images are more visually acceptable and the cold inserts are better defined. However, no additional rod segments or spheres can be visualized post-FBNR.

Evaluation of clinical data

FBNR, median-filtered and raw vertex-view DaTSCAN images are shown in Fig. 7. Good qualitative results were realized for the FBNR processed image compared with the over-smoothed median-filtered and noisy raw data.

The qualitative degradation of the half-count MPS dataset can be seen in Fig. 8a, making visual interpretation harder, particularly for defects along the vertical and horizontal long axis, where additional probable defects were reported in the apex, anterior wall and septum when using the half-count data. A single possible additional defect was reported post-application of FBNR.

Conclusion

An adaptive noise-reduction filter, which explicitly utilizes the Poisson nature of noise encountered in scintigraphic imaging, has been developed and evaluated using simulated and clinical nuclear medicine images. As the FBNR algorithm is reliant on the Poisson nature of counting statistics within the dataset, any significant change to the count distribution by, for example, the application of a uniformity correction map, may affect the quality of the result. However, the addition and/or subtraction of pixel counts through correction maps will also alter the frequency information within the image and degrade conventional filtering techniques. The noise present in one of the phantom distributions used to evaluate FBNR was verified experimentally to be of Poisson distribution. Therefore, it is felt unlikely that correction maps significantly degrade FBNR. However, care should be taken to experimentally evaluate FBNR, or any Poisson noise correction algorithm, on each gamma camera system, particularly systems that require extensive uniformity correction.

No additional image artefacts were seen post-application of FBNR in the simulated, experimental and clinical datasets studied. MNE values indicate FBNR processing is equivalent to obtaining a raw image with between 2.5 and 10 times the number of counts for the range of phantoms studied.

References

1 Bonnin F, Buvat I, Benali H, Di Paola R. A comparative study of scatter correction methods for scintigraphic images. *Eur J Nucl Med* 1994; **21**:388–393.

2 Fleming JS. A technique for using CT images in attenuation correction and quantification in SPECT. *Nucl Med Commun* 1989; **10**:83–97.

3 Kessler RM, Ellis JR, Eden M. Analysis of emission tomographic scan data: limitations imposed by resolution and background. *J Comput Assist Tomogr* 1984; **8**:514–522.

4 Germano G, China T, Kavanagh PB, Kiat H, Berman DS. Detection and correction of patient motion in dynamic and static myocardial SPECT using a multidetector camera. *J Nucl Med* 1993; **34**:1349–1355.

5 Tsui BMW, Beck RN, Doi K, Metz CE. Analysis of recorded image noise in nuclear medicine. *Phys Med Biol* 1981; **26**:883–902.

6 Metz CE, Beck RN. Quantitative effects of stationary linear image processing on noise and resolution of structure in radionuclide images. *J Nucl Med* 1974; **15**:164–170.

7 King MA, Penney BC, Glick SJ. An image dependent Metz filter for nuclear medicine images. *J Nucl Med* 1988; **29**:1980–1989.

8 Penney BC, King MA, Schwinger RB, Baker SP, Stritzke P, Doherty PW. Constrained least-squares restoration of nuclear medicine images: selecting the coarseness function. *Med Phys* 1987; **14**:849–858.

9 Hull DM, Peskin CS, Rabinowitz AM, Wexler JP, Blaufox MD. The derivation and verfication of a non-stationary, optimal smoothing filter for nuclear medicine image data. *Phys Med Biol* 1990; **35**:1641–1662.

10 Hannequin P, Mas J. Statistical and heuristic image noise extraction (SHINE): a new method for processing Poisson noise in scintigraphic images. *Phys Med Biol* 2002; **47**:4329–4344.

11 Lee JS. Speckle analysis and smoothing of synthetic aperture radar images. *Comput Graph Image Process* 1981; **17**:24–32.

12 Guy MJ, Flux GD, Papavasileiou P, Flower MA, Ott RJ. RMDP: a dedicated package for iodine-131 SPECT quantification, registration, patient-specific dosimetry. *Cancer Biother Radiopharm* 2003; **18**:61–69.